

Strange hyperon and antihyperon production from quark and string-rope matter

P. Csizmadia¹, P. Lévai^{1,2*}, S.E. Vance²,
T.S. Biró¹, M. Gyulassy², J. Zimányi¹

¹ KFKI Research Institute for Particle and Nuclear Physics,
P. O. Box 49, Budapest, 1525, Hungary

² Department of Physics, Columbia University,
New York, NY, 10027, USA

18 September 1998

Abstract

Hyperon and antihyperon production is investigated using two microscopical models: (1) the fast hadronization of quark matter as given by the ALCOR model; (2) string formation and fragmentation as in the HIJING/B model. We calculate the particle numbers and momentum distributions for Pb+Pb collisions at CERN SPS energies in order to compare the two models with each other and with the available experimental data. We show that these two theoretical approaches give similar yields for the hyperons, but strongly differ for antihyperons.

1 Introduction

The quest to produce the Quark-Gluon Plasma (QGP) at the CERN SPS has reached its final stage with the Pb+Pb run at $E_{beam} = 158$ AGeV. Since strangeness enhancement in heavy ion collisions relative to pp collision has been predicted as a QGP signal [1, 2], the measurement of strange and antistrange particles, especially the hyperons and the antihyperons, has received much attention (see Refs. [3]-[11]). Several thermal models were invented to reproduce earlier experimental data at the AGS and the SPS energies [12, 13, 14]. However, only extended versions which introduce more parameters are capable of fitting the new experimental data which particularly include the hyperon and antihyperon yields [15]. Although these thermal models are capable of describing the gross yields and thermodynamic properties which are observed in the final state of the collisions, they are unable to provide a description of the various underlying microscopical mechanisms which

*Talk given at the 4th Int. Conference on Strangeness in Quark Matter, July 20-24, 1998, Padova, Italy, submitted to J. Phys. G.

may be involved in the initial stages following the collision of the two nuclei. Thus, to test for the formation of a QGP or any other possible initial phase, we choose two microscopical models which describe the evolution of heavy ion collisions from two different viewpoints; a plasma vs. a hadronic scenario.

The first model assumes the formation of a deconfined state (namely the Constituent Quark Plasma (CQP) [16, 17]) and then describes its hadronization. The applied ALgebraic Coalescence Rehadronization (ALCOR) model [18, 19] and MICROscopical Coalescence Rehadronization (MICOR) model [20] (as well the time-dependent Transchemistry Model [16, 17]) are all based on this assumption.

The second model begins with a description of hadron-hadron collisions using string phenomenology. The strings are then fragmented to produce the final observed hadron spectrum. The HIJING/B [21] event generator (an extension of HIJING [22] event generator to include a baryon number transport mechanism) is one version of this model. The Relativistic Quantum Molecular Dynamics (RQMD) model is another variant of this model [23]. However, we note that HIJING and HIJING/B greatly differ from RQMD in that they include minijets.

Although both of these models are able to reproduce pion, kaon and proton data, they differ in their predictions of the hyperons and the antihyperons. Thus the underlying assumptions of these models can be investigated by comparing their theoretical predictions for the hyperon and the antihyperon production with the experimental data.

Before discussing our calculations, we argue that secondary hadronic collisions negligibly effect the measured hadronic spectra at SPS energies. We note that secondary hadronic interactions are needed to describe the lower energy heavy ion collisions (at SIS and AGS) as seen in the successful use of hadronic cascade models in reproducing data at these energies. However, at $E_{beam} \approx 100\text{-}200$ GeV/nucleon we expect that the collisions involve the quarks of the nucleon. This introduces uncertain hadronic formation time with the production of a hadron from the intermediate quark matter or string/rope resonance. This time is on the order of the life-time of the early highly excited system. This idea is just the old argument given by Pomeranchuk and Feinberg [24] who claimed that particles only really materialize, not at the early collision stage, but at low energy densities where they freeze-out and become interactionless; the “free separation” of particles.

The HIJING and HIJING/B models use this assumption, since fragmentation occurs after the nuclei have finished colliding. (We will also display the ‘no-scattering’ results of RQMD from Ref. [23].)

The ALCOR and MICOR models assume that the hadronization of deconfined matter yields an excited hadronic gas which includes excited resonances, namely the vector meson nonet and the baryon decuplet beyond the lowest lying pseudoscalar nonet and baryon octet. The resonances decay into the stable hadrons. All of these models, except RQMD neglect final state interactions.

Since the final hadron production of these models is directly related to the underlying microscopical mechanisms, we compare their predictions of hyperon and antihyperon formation with each other and with the available experimental data.

2 The ALCOR and MICOR models

In Pb+Pb collisions at the CERN SPS energies, it is assumed that the incoming nucleons disintegrate into a form of deconfined matter. Originally the appearance of the perturbative QGP phase was expected. However, around the critical temperature, $T_c \approx 150 - 200$ MeV, perturbative QCD is unable to describe the characteristic processes completely, thus non-perturbative or phenomenological descriptions should be introduced for the deconfined matter. The non-perturbative descriptions can be motivated by lattice QCD calculations of the equation of state near critical temperature T_c . Recent analysis indicates [25] that deconfined matter in its equilibrium state can be described by massive quarks and gluons. These gluon-like quasi-particles are heavier than the quarks (thus their number is suppressed if the system is thermalized) and the effective quark masses are close to the constituent quark masses of the additive quark model [26]. We call this deconfined state the Constituent Quark Plasma (CQP). The CQP state is dominated by quarks and antiquarks, where some combine to form colorless hadron-like objects. The presence of such prehadrons in the deconfined phase is confirmed by lattice-QCD calculations of hadronic correlation functions [27]. It is assumed that these prehadrons can escape from the strongly interacting region to become mostly excited “real” hadrons.

The ALCOR model describes this microscopical hadronization process using quark coalescence (for a detailed description see Refs.[18, 19]). The coalescence rates depend on the temperature T , on the thermal quark masses M_q and M_s , and on the strength of the coalescence, which can be characterized by an effective α_{eff} coupling in a Coulomb-like quark-quark interaction potential. From the point of view of hyperon and antihyperon production it is important to note, that the applied coalescence cross section is proportional to the mass of produced prehadron, $\sigma_{coal}^{i+j \rightarrow h} \propto m_h^2$ (see Ref. [18]). Thus the production of heavier particles, especially the hyperons (antihyperons) containing the heavy strange quark (antiquark) is relatively enhanced. To describe the hadron formation completely, two more parameters are needed: the number of newly produced light quarks $N_{q\bar{q}} = N_{u\bar{u}} = N_{d\bar{d}}$ and number of strange quarks $N_{s\bar{s}}$. The values of $N_{q\bar{q}}$ and $N_{s\bar{s}}$ are scaled by A^β , where $\beta \approx 1$. These input parameters, combined with some initial geometry and a longitudinal Bjorken scaling are the basis of the ALCOR model which calculates the total number of produced hadrons for different heavy ion collisions.

In the ALCOR model the coalescence rates are determined from multidimensional integrals which can be calculated exactly for the case of Bjorken scaling. To obtain the differential momentum spectra of the produced hadrons, integrals need to be separated and differential coalescence rates need to be evaluated numerically. The introduction of numerical integrals allows us to consider a more complicated flow pattern, in the present case a constant transverse flow characterized by v_{tr} , and a finite longitudinal extension characterized by the maximal space-time rapidity η_{max} . A new version of the ALCOR model, the Microscopical Coalescence Rehadronization (MICOR) model [20], includes this new flow pattern and calculate the differential momentum spectra. Here, the microscopical quark coalescence produces off-shell prehadrons and we assume that these prehadrons escape the deconfined region conserving their velocity to become real on-shell hadrons. (Because of the small deviation between prehadron and real hadron masses, this assumption works well.) After calculating the differential rates, the absolute norms of the particle production are determined by a set of equations based on quark and antiquark number

conservation, similarly to ALCOR. The MICOR model is able to determine the differential hadron spectra which arises from the hadronization of the CQP state. As in ALCOR, final state hadronic rescattering is neglected.

The advantage of using the ALCOR and MICOR models is that the phase transition can be followed microscopically. In this way a phenomenological quark-quark interaction determines the formation of a chemically out-of equilibrium hadronic gas.

3 The HIJING/B model

As has been summarized elsewhere [22], the HIJING Monte Carlo event generator models hadronic interactions by combining low p_T multistring phenomenology with the perturbative QCD (pQCD) processes. The HIJING/B [21] event generator extends the HIJING model by introducing a novel, non-perturbative gluon junction mechanism in order to study baryon number transport in heavy-ion collisions. As shown below, this novel non-perturbative junction mechanism strongly influences hyperon production.

This gluonic mechanism is motivated from the non-perturbative gluon field configuration (the baryon junction) that appears when writing the simplest gauge invariant operator for the baryon in $SU_c(3)$;

$$\begin{aligned}
 B &= \epsilon^{ijk} \left[P \exp \left(ig \int_{x_1}^{x_J} dx^\mu A_\mu \right) q(x_1) \right]_i \\
 &\times \left[P \exp \left(ig \int_{x_2}^{x_J} dx^\mu A_\mu \right) q(x_2) \right]_j \left[P \exp \left(ig \int_{x_3}^{x_J} dx^\mu A_\mu \right) q(x_3) \right]_k. \quad (1)
 \end{aligned}$$

Here, the baryon junction is the vertex at x_J where the three gluon Wilson lines link the three valence quarks to form the gauge invariant non-local operator. In a highly excited baryonic state, the Wilson lines represent color flux tubes. When these strings fragment via $q\bar{q}$ production, the resulting baryon will be composed of the three sea quarks which are linked to the junction while the original valence quarks will emerge as constituents of three leading mesons. Being a gluonic configuration, it was proposed [28] that the junction could be easily transported into the mid-rapidity region in hadronic interactions.

In Regge phenomenology, allowing for the possibility of baryon junctions in scattering is taken into account by introducing additional Regge trajectories (M^J). As was shown by Kharzeev [28], the exchange of these trajectories in $p + p$ interactions leads to events where one of the baryon junctions is stopped in the mid-rapidity region. Once the baryon junction is stopped, the three valence quarks continue forming three beam jets. These events have a different energy, rapidity and multiplicity dependence compared to the normal Pomeron two string event. In particular, the produced baryon has a $\cosh(y/2)$ rapidity dependence and a $1/\sqrt[4]{s}$ energy dependence. In addition, the new string configuration leads to a multiplicity enhancement of a factor of 5/4 (counting the two + three jets as compared with the two + two jets). Since the baryon which is resolved around the junction in the mid-rapidity region is composed of three sea quarks, hyperon production and the $\langle p_t^2 \rangle$ of the final baryon are enhanced by factors of 3. The enhancement factor of 3 of the strangeness content of the baryon allows for the unique possibility of producing Ω^- ($S = -3$) baryons.

In HIJING/B [21], the baryon junction mechanism is implemented using a “Y” string configuration for the excited baryon with an effective cross section of ~ 9 mb. The above junction dynamics does not provide a mechanism for antibaryons production and further studies which address baryon pair production are underway. In their present version, neither HIJING nor HIJING/B include final state interactions. Thus, in one variant of HIJING/B we simulate multiple final state interactions using the concept of “ropes” [29]; increasing the energy per unit length of the strings from 1.0 GeV/fm to 1.45 GeV/fm in the heavy nuclear collisions. Increasing the effective string tension increases the strangeness production and the $\langle p_T \rangle$.

4 Results on PbPb collision

In the ALCOR model, we recalculate the hadron production as compared with earlier publications [18, 19]. In this calculation, we considered the feeding of the detected Λ s from Ξ and Ω decay channels and the undistinguishable Σ^0 . We also introduce the Λ^0 -like $\equiv \Lambda^0 + \Sigma^0 + \Xi^- + \Xi^0 + \Omega^-$ species, which was not done earlier. This number will be compared to the experimentally measured number of “ Λ ”-particles, as was done similarly with “ $\bar{\Lambda}^0$ -like” particles. In this case the input parameters for newly produced quark pairs are $N_{q\bar{q}} = 391$ and $N_{s\bar{s}} = 172$ (which means $g_s = N_{s\bar{s}}/(N_{u\bar{u}} + N_{d\bar{d}}) = 0.22$) and for the effective quark-quark interaction, $\alpha_{eff} = 0.97$. The results are displayed in Table 1.

The particle yields were also calculated in HIJING/B with ropes where the energy per unit length of the string was increased to $\kappa = 1.45$ GeV/fm. The total numbers are shown in Table 1 along with the RQMD results [23].

When comparing the two calculations, ALCOR and HIJING/B predict approximately the same numbers of mesons, baryons and non-strange antibaryons; approximately reproducing the experimental data. However, significant differences can be seen in the predictions of strange antibaryons and the Ω . These differences are directly related to the assumed microscopical hadronization mechanisms and thus reveal the applicability of the different assumptions. These differences can be investigated via particle ratios, which are displayed in Table 2 and 3. In Table 2 and in Table 3, the experimental results obtained from NA49 Collaboration and the WA97 Collaboration are shown, respectively. We note that these measured ratios are valid in certain rapidity windows, and thus only provide an approximate comparison.

We also investigate the energy dependence of our results. Particle abundances were calculated at 100, 200 and 300 AGeV for Pb+Pb collisions using HIJING/B with ropes and the ALCOR model. In the ALCOR model we kept the g_s and α_{eff} parameters at their value obtained by fitting the data at 158 AGeV, and only changed the number of newly produced light quarks, $N_{q\bar{q}} = 354, 442, 496$, respectively, to reproduce the h^- number as obtained in HIJING/B. The results of the energy dependence of strange particle ratios from these calculations are shown in Figure 1. In addition, we show the experimental results from the NA49 and WA97 experiments. Although both models reveal a slight energy dependence, only the ALCOR model was able to consistently reproduce the observed values.

Pb+Pb	NA49	ALCOR	HIJING/B	RQMD
h^-	680 ^a	679.8	700.8	829.2
π^+		590.6	608.7	692.9
π^0		605.9	622.8	724.9
π^-		622.0	636.9	728.8
K^+	76*	78.06	79.4	79.0
K^0		78.06	79.4	79.0
\bar{K}^0		34.66	35.2	50.4
K^-	{32} ^b	34.66	35.2	50.4
p^+		153.2	152.3	199.7
n^0		170.5	165.2	217.6
Σ^+		9.16	12.3	12.9
Σ^0		9.76	11.8	13.1
Σ^-		10.39	12.4	13.3
Λ^0		48.85	40.2	35.3
Ξ^0		4.89	4.90	4.2
Ξ^-	7.23 ± 0.88^d	4.93	4.93	4.2
Ω^-		0.62	0.43	
\bar{p}^-		6.24	9.67	27.9
\bar{n}^0		6.24	9.62	27.9
$\bar{\Sigma}^-$		0.91	1.33	4.6
$\bar{\Sigma}^0$		0.91	1.19	4.6
$\bar{\Sigma}^+$		0.91	1.17	4.6
$\bar{\Lambda}^0$		4.59	2.84	10.7
$\bar{\Xi}^0$		1.12	0.44	2.0
$\bar{\Xi}^+$	$\{1.6 \pm 0.2\}^d$	1.12	0.44	2.0
$\bar{\Omega}^+$		0.35	0.012	
K_S^0	{54} ^{b,c}	56.36	57.3	63.5
$p^+ - \bar{p}^-$	{145} ^a	147.03	142.6	171.8
Λ^0 -like	$\{49 \pm 6\}^d$	69.07	62.31	56.8
$\bar{\Lambda}^0$ -like	$\{8.8 \pm 1.0\}^d$	8.12	4.92	19.3

Table 1: Total hadron multiplicities for $Pb + Pb$ collision at bombarding energy 158 GeV/nucleon. The displayed experimental results are obtained or estimated ($\{\}$) from the publications of NA49 Collaboration: ^a is from [10]; ^b is from [7]; ^c is from [11]; ^d is from [3]; * is estimated from $\{K^-\}$ and $\{K_S^0\}$. Theoretical results are calculated in the ALCOR and HIJING/B models and it was included the results of RQMD model ("ropes + no re-scattering" version) [23]. We introduced Λ^0 -like $\equiv \Lambda^0 + \Sigma^0 + \Xi^- + \Xi^0 + \Omega^-$.

Pb+Pb	NA49	ALCOR	HIJING/B	RQMD
Ξ^+/Ξ^-	0.232 ± 0.033	0.227	0.089	0.476
$\Xi^+/\bar{\Lambda}$	0.188 ± 0.039	0.138	0.089	0.103
Ξ^-/Λ	0.148 ± 0.011	0.071	0.078	0.074

Table 2. Strange baryon and antibaryon ratios measured by NA49 Coll. [3] for $Pb + Pb$ collision at 158 GeV/nucleon bombarding energy in the momentum region $3.1 \geq y \geq 4.1$, $p_T > 0$. We calculated the ratios of total numbers from Table 1. Here $\Lambda(\bar{\Lambda})$ means “ Λ^0 -like” (“ $\bar{\Lambda}^0$ -like”) species.

Pb+Pb	WA97	ALCOR	HIJING/B	RQMD
$\bar{\Lambda}/\Lambda$	0.128 ± 0.012	0.117	0.079	0.339
Ξ^+/Ξ^-	0.266 ± 0.028	0.227	0.089	0.476
$\bar{\Omega}^+/\Omega^-$	0.46 ± 0.15	0.564	0.028	—
Ξ^-/Λ	0.093 ± 0.007	0.071	0.079	0.073
$\Xi^+/\bar{\Lambda}$	0.195 ± 0.023	0.138	0.089	0.103
Ω^-/Ξ^-	0.195 ± 0.028	0.125	0.087	—

Table 3. The ratios of strange baryons and antibaryons, measured by the WA97 Collaboration [6] for $Pb + Pb$ collision at 158 GeV/nucleon bombarding energy at $p_T > 0$ GeV. We calculated the ratios of total numbers from Table 1. Here $\Lambda(\bar{\Lambda})$ means “ Λ^0 -like” (“ $\bar{\Lambda}^0$ -like”) species.

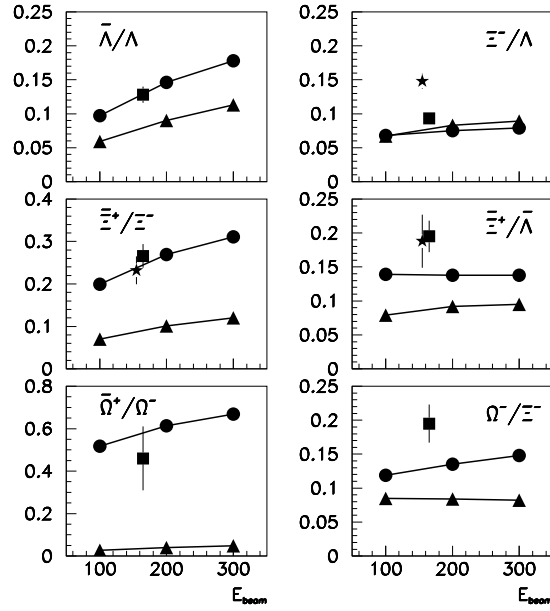


Figure 1. The measured ratios of baryons and antibaryons in the PbPb collision at 158 AGeV energy from the NA49 Coll. (stars) [3, 10] and the WA97 Coll. (squares) [6]. The theoretical results from ALCOR (dots) and HIJING/B (triangles) are displayed at 100, 200 and 300 AGeV energy.

The transverse momentum distributions of the produced hadrons in the mid-rapidity region were also calculated using the MICOR model. For this calculation, two initial conditions were considered. Since the ALCOR model is not very sensitive to the initial temperature T_{CQP} , in the range $150 \text{ MeV} < T_{CQP} < 180 \text{ MeV}$, two set of parameters were used in the MICOR calculation: I. $T_{CQP} = 150 \text{ MeV}$, $v_{tr} = 0.67$; II. $T_{CQP} = 175 \text{ MeV}$, $v_{tr} = 0.57$. In case I, the pion and proton spectra is reproduced at midrapidity. In case II, good agreement was found for the heavier hyperons.

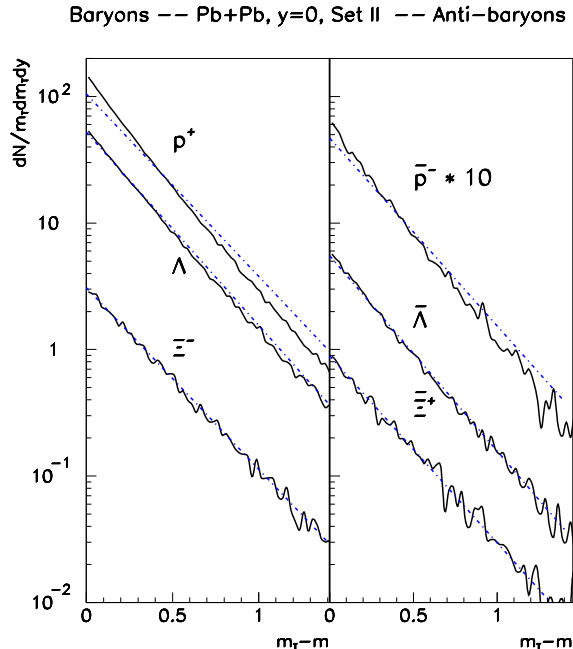


Figure 2. The transverse momentum distribution of proton, Λ , Ξ^- and their antiparticles in Pb+Pb collision in midrapidity, produced by the MICOR model with initial condition set II. The full curves are the results of calculation and the dashed lines indicate experimental slopes measured by NA49 Coll. [3].

In the MICOR model, the non-thermal momentum distributions of the emerging excited hadrons can be calculated. These distributions can be characterized by a non-Boltzmann distribution, $f \propto (m/E)^\delta \cdot \exp(-E/T)$, where $\delta \approx 2$. What is remarkable is that after resonance decay the obtained hadronic spectra can be very well fitted by pure exponential functions [20], with the effective slopes closely matching the experimental values. In Figure 2, we display the resulting momentum spectra using the values from case II for the proton, Λ , Ξ^- and their antiparticles. Here, the solid lines show the MICOR results, which can be parametrized by the exponential fit:

$$\frac{dN}{m_T dm_T dy} = C \cdot e^{-m_T/T_{eff}} . \quad (2)$$

These results can be compared to the dashed lines which represent the slopes as measured by the NA49 Collaboration [3, 4]. Here, we show that after two completely non-equilibrium steps (quark coalescence and decay of excited hadrons) the final hadron

spectra is approximately exponential. Our result in Figure 2 demonstrates that non-equilibrium processes are able to produce particle spectra which can also be interpreted as thermal. We note that baryons and antibaryons have approximately the same slope, as has been observed.

In Figure 3, we display the effective slopes T_{eff} as calculated using the MICOR model (using cases I and II) and as measured by the NA49 [3, 4], NA44 [9] and WA97 Collaborations [6, 8]. The possible interpretation of our MICOR results is the following: parameter sets I and II are so close to each other that a mutual hadronization temperature and transverse flow inbetween (namely $T_{CQP} \approx 170 MeV$ and $v_{tr} \approx 0.6$) could be assumed for the produced deconfined state as the dotted line shows in Figure 3 (see Ref. [3]). The deviation of the recent experimental data from this line indicates that hyperons (antihyperons) which contain mostly strange (antistrange) quarks escaped the light-quark dominated CQP state at a slightly earlier time, when the temperature is higher and the transverse flow is smaller. Particles containing mostly light quarks are formed in the later stage of the expanding CQP matter and thus their spectra indicate a lower temperature but higher transverse flow upon hadronization. We note that there is a similar, interacting hadronic explanation [30] which was obtained from an RQMD-based analysis which assumes secondary interactions with different strengths for strange and non-strange particles. We hope that final data on Ω^- and $\bar{\Omega}^+$ production will help us to make our conclusion more definite.

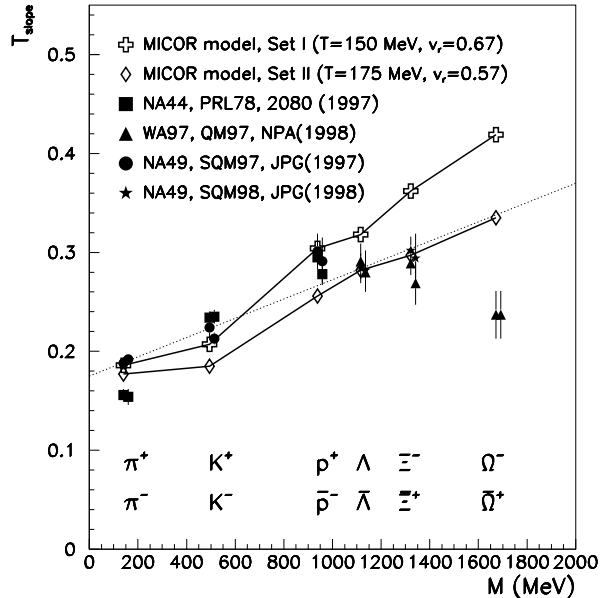


Figure 3. The effective slope parameters, T_{eff} , in the midrapidity region for Pb+Pb collision at 158 AGeV, obtained from the MICOR model and from the different experiments. The dotted line indicates the appearance of a common transverse flow in the hadronic phase, see Ref. [3].

5 Conclusion

We investigate hyperon and antihyperon production in Pb+Pb collision at CERN SPS energies using two different scenarios. The formation of a Constituent Quark Plasma and the modeling of its hadronization as in the ALCOR and MICOR models was used to calculate the particle numbers and transverse momentum distributions. String formation and fragmentation as in the HIJING/B with ropes model was also used to calculate particle yields. In the case of meson, baryon and non-strange antibaryon yields, both models predict similar particle numbers. However, only the CQP scenario could reproduce the antihyperon data. This can be attributed to the coalescence of heavier strange quarks which is favoured in the ALCOR model. The inability of HIJING/B to reproduce the antihyperon data reveals the need for a new hadronic mechanisms (similar to the baryon junction) for antihyperon production.

In addition to reproducing the antihyperon yields, the results of the CQP-based MICOR model point to a scenario where a mutual transverse flow was developed in the deconfined phase and that hadronization occurred when $T_{CQP} \approx 170$ MeV and $v_{tr} \approx 0.6$. Here, hyperons and antihyperons may escape a little bit earlier from the deconfined region, retaining a slightly larger temperature and a smaller collective transverse flow. The other hadrons are then formed shortly thereafter.

Acknowledgments

One of us (P.L.) thanks for M. Morando for the kind hospitality at Padova and for F. Grabler and S. Margetis to make available their contribution before submission. One of us (M.G.) is grateful to the KFKI RMKI for its hospitality during the course of this work. This work was supported by the Hungarian Science Fund (OTKA) grants T024094 and T025579 and by the US-Hungarian Science and Technology Joint Fund No. 652/1998.

References

- [1] T. S. Biró and J. Zimányi, Phys. Lett. B **113**, 6 (1982); Nucl. Phys. **A395**, 525 (1983).
- [2] J. Rafelski, B. Müller, Phys. Rev. Lett. **48**, 1066 (1982); P. Koch, B. Müller, and J. Rafelski, Phys. Rep., **C142**, 167 (1986).
- [3] F. Grabler for NA49 Coll., SQM'98, these proceedings.
- [4] S. Margetis for NA49 Coll., SQM'98, these proceedings.
- [5] R. Lietava for WA97 Coll., SQM'98, these proceedings.
- [6] I. Kralik et al., WA97 Coll., Nucl. Phys. **A638**, 115c (1998).
- [7] C. Bormann for the NA49 Coll., J. of Phys. **G23**, 1817 (1997).
- [8] A.K. Holme et al., WA97 Coll., J. of Phys. **G23**, 1851 (1997).

- [9] I.G. Bearden et al., NA44 Coll., Phys. Rev. Lett. **78**, 2080 (1997)
- [10] S.V. Afanasiev et al., NA49 Coll., Nucl. Phys. **A610**, 188c (1996).
- [11] S. Margetis for the NA49 Coll., Heavy Ion Phys. **4**, 63 (1996).
- [12] J. Letessier, A. Tounsi, U. Heinz, J. Sollfrank, J. Rafelski, Phys. Rev. D **51**, 3408 (1995).
- [13] P. Braun-Munzinger, J. Stachel, J.P. Wessels, N. Xu, Phys. Lett. B **344**, 43 (1995); ibid. B **365**, 1 (1996); P. Braun-Munzinger and J. Stachel, Nucl. Phys. A **606**, 320 (1996).
- [14] J. Sollfrank, J. Phys. G **23**, 1903 (1997); J. Sollfrank, F. Becattini, K. Redlich, H. Satz, Nucl. Phys. A **638**, 399c (1998).
- [15] J. Letessier, J. Rafelski, hep-ph/9807346; and these proceedings.
- [16] J. Zimányi, T.S. Biró, and P. Lévai, J. Phys. **G23**, 1941 (1997); T. S. Biró, P. Lévai, and J. Zimányi, submitted to Phys. Rev. C, hep-ph/9807303; T. S. Biró, P. Lévai, J. Zimányi, and C.T. Taxler, hep-ph/9808394.
- [17] T. S. Biró, P. Lévai, and J. Zimányi, these proceedings, (talk of J. Zimányi), hep-ph/9809385;
- [18] T. S. Biró, P. Lévai, and J. Zimányi, Phys. Lett. B **347**, 6 (1995).
- [19] J. Zimányi, T. S. Biró, T. Csörgő, and P. Lévai, Heavy Ion Phys. **4**, 15 (1996).
- [20] P. Csizmadia, P. Lévai, J. Zimányi, Proc. of the XXV. Int. Workshop on Gross Properties of Nuclei and Nuclear Excitations, Hirschegg, 1997; P. Csizmadia, P. Lévai, in preparation.
- [21] S.E. Vance, M. Gyulassy and X.N.. Wang, submitted to Phys. Lett. **B**, nucl-th/9806008.
- [22] X. N. Wang and M. Gyulassy, Phys. Rev. **D44** (1991) 3501; Phys. Rev. **D45** (1992) 844; Comp. Phys. Comm. **83** (1994) 307.
- [23] H. Sorge, Phys. Rev. C **52**, 3291 (1995); Nucl. Phys. A **590**, 571c (1995).
- [24] I. Ya. Pomeranchuk, Dokl. Akad. Sci USSR **78**, 884 (1951); E.L. Feinberg and I.Ya. Pomeranchuk, Suppl. Nuovo Cimento **3**, 652 (1956); Phys. JETP **23**, 132 (1966);
- [25] P. Lévai and U. Heinz, Phys. Rev. C **57**, 1879 (1998).
- [26] A. de Rujula, H. Georgi, S.L. Glashow, Phys. Rev. **D12**, 147 (1975).
- [27] K.D. Born et al., MTC Coll., Phys. Rev. Lett. **67**, 302 (1991).
- [28] D. Kharzeev, Phys. Lett. **B378**, 238 (1996), nucl-th/9602027.
- [29] T.S. Biro, H.B. Nielsen, and J. Knoll, Nucl. Phys. B **245**, 449 (1984).
- [30] H. van Hecke, H. Sorge, N. Xu, nucl-th/9804035.